2024 IEEE/RSJ International Conference on Intelligent Robots and Systems (IROS)
October 14-18, 2024. Abu Dhabi, UAE

Preliminary Result of Cury: A Backdrivable Leg Design using Linear Actuators

Zhongtao Guan, Yiming Chen, Junlei Zhu, Yu Hu, Weibang Bai, and Jiahao Chen*

***Abstract*— This paper reports the design, simulation, and experiment of a robotic leg prototype named Cury, which has the potential to achieve minimal clearance and excellent backdrivability. Inspired by human walking data, the actuator design incorporates four-bar linkages and ball screws, and is further optimized to meet the torque requirement. The Webots simulation is used to obtain the closed-loop chain description of the robotic leg from fits URDF specification, and this simulation is used to assess the actuator output requirements at a given predefined trajectory. Leveraging customized ac motors and drives, Cury demonstrates satisfactory trajectory tracking performance using a simple controller. The motor drive design files and Webots simulation files are open-sourced.**

Keywords: bipedal robot, linear actuator, mechatronics.

I. Introduction

Legged robots, especially bipedal robots, have great potential for athletic abilities and agile movement [1]–[6]. We have seen electric actuation has prevailed for its simple structure, as it eliminates the placement of the pipelines needed for hydraulic actuation. However, the ac motor, as the key component of electric actuation, is not suitable for robotic joint application and planetary gearbox or harmonic drive is often needed to amplify the output torque of the ac motor [7], [8]. The mechanical gearbox impairs the backdrivability of the actuator and inevitably introduces clearance in its mechanical transmission. Clearance deteriorates controller performance [9], imposes requirements for additional joint encoders and force sensors, and even causes mechanical damage in contact impact events such as fast leg movement [10].

Direct-drive (DD) robots have advantages in terms of backdrivability, small clearance, high control bandwidth [11]. Robots based on DD actuators can be greatly simplified, making the system more robust and better suited for agile movements and complex dynamics. However, this kind of actuator design usually requires a high torque density motor to work at a low speed and high torque conditions, which often deviates from motor's high efficiency operating range. To improve the operating condition of the motor while maintaining the advantage of DD, the quasi-direct-drive (QDD) has been proposed as an idea of using a small reduction ratio gearbox or belt [12]–[15].

All the designs of actuators discussed so far have a constant reduction ratio. According to data measured from humans [16], [17], it can be concluded that torque requirement during bipedal robot walking and jumping varies in a nonlinear manner with respect to the joint angle, and results in fluctuation in the motor's power output during motion. Additionally, static friction of gearboxes or belts in QDD inevitably increases start torque (as compared to DD), leading to a hysteresis band when changing rotating direction, which make it difficult to control.

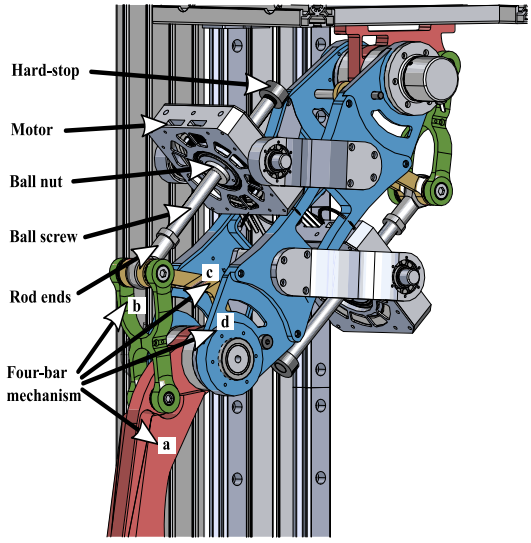

Fig. 1. The leg prototype Cury is tested on the test bench.

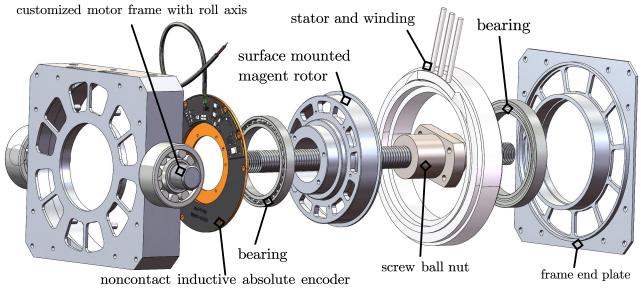

Fig. 2. Exploded view of the F130-16-KV20 motor model with the ball screw.

This paper presents a two-degree-of-freedom (DoF) leg prototype named Cury for making a bipedal robot. In order to offer torque amplification while maintaining the joint's backdrivability, Cury employs a high-lead ball screw, of which a prior design can be found in [18]. A set of four-bar linkages is added to the ball screw end of the leg to give enough torque across the joint motion range, enabling a dynamic reduction ratio at both hip joint and knee joint, as shown in Fig. 1, where different colors correspond to different linkages in the four-bar mechanism. This paper further defines a multi-objective optimization problem to determine the location of the motor and the length of four-bar links, taking human walking data (see, e.g., [17]) into account.

The electrical system for Cury mainly consists of an ac motor drive that can provide two kilowatt of electrical power to the two motors with a single microcontroller. This motor drive is also strong in scalability as it reserves interfaces for multiple communication protocols and only requires the replacement of a few components to drive motors with different power requirements.

An precise system model is required to replicate the movements of the robotic leg in simulation. The four-bar links form a closed-loop chain, which has proven to be a major challenge to simulate because the closed-loop chain exhibits much more intricate dynamics as compared to an open kinematic tree and requires additional constraints for loop closure [19]. The unified robot description format (URDF) describes robot as a tree that only allows a unique link between any two nodes thus it cannot describe closed-loop chains. Although other format such as Simulation Description Format (SDF) and MJCF support closed-loops chain, it is hard to obtain from CAD design softwares such as Solidworks. Our attempt to model a closed-loop chain four-bar linkage has been successful with Webots [20], which is found to be able to simplify the process of converting the CAD model to simulation and well support simulation of a mechanical closed-loop chain. The hardware designs, including PCB files, schematics and the firmware and our Webots simulation have been open-sourced.[1]

II. Hardware Design

Cury, shown in Fig. 1, is a two-DoF leg prototype with a four bar mechanism that mimics a bionic joint, as has been seen in powered prosthesis [21] and Tesla Optimums [5]. Its thigh and shank are both approximately 400 mm in length. The two linear actuators are identical in mechanical design for ease of fabrication, and they are positioned on both sides of the thigh in a center symmetric manner.

Each linear actuator consists of one three-phase ac motor, a '1616' ball-screw[2], screw ball-nut, screw hard-stop, eye-shaped rod end, a group of four-bar linkages, two pairs of thrust bearings and deep groove ball bearings. In virtue of the actuator design, Cury can control ground reaction force by directly controlling the motor current without any extra force sensor, and it has the potential to obtain the joint's angular position without needing a joint encoder.

A. Motor

The motor we use is the F130-16-KV20 model[3] from Pan Motor [22], and it is an inner-rotor surface-mounted permanent-magnet synchronous motor, with customized stator frame that provides the roll-axis on the motor holder in the assembly of Cury. Fig. 2 shows the exploded view of the customized motor. The motor is equipped with a hollow, non-contact inductive absolute encoder with a resolution of 23 bit. The motor features a high slot copper fill ratio as its stator is wired by an industrial robot that applies proper tension during the whole wiring process. The motor has 52 rotor magnet poles and 48 stator slots. The high slot number design allows the stator iron core to have shorter stator tooth and hence larger air gap radius, which generally improves the torque density since the Maxwell shear stress is integrated over the air gap surface area of the rotor cylinder to produce torque.

B. Mechanical Design

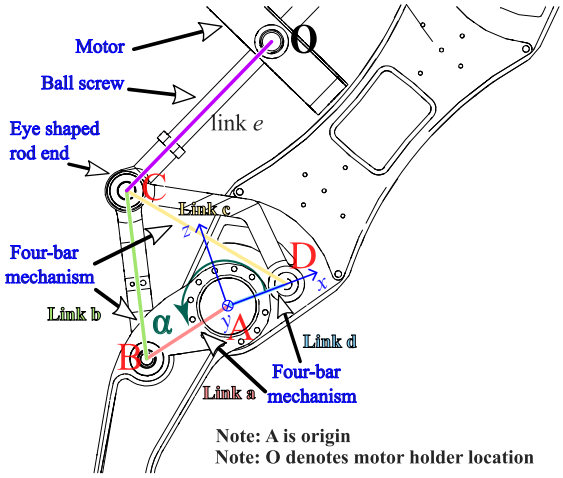

Fig. 3. Symbol definitions and annotations of the four-bar linkage, using the shank actuator as an example. Big capital denotes the end of each bar, while small capital denotes the links.

The four-bar mechanism introduces a dynamic reduction gain and a variable lever arm, which is found to effectively transmit motor torque to output joint. The curved link c (see Fig. 3) is designed to increase the motion range of the joint. The ball screw is used to transform the motor rotation into linear motion and to push the four-bar linkage. The off-shelf rod end product is attached to the end of the ball screw but it provides an undesired extra degree of freedom of rotation. We add two additional 3D printed parts to the both sides of the rod end to eliminate such rotation.

To balance between the speed and output torque while achieving backdrivability and transmission efficiency of the joints, the ball-screw is chosen to have a large lead angle of 17.7 deg, which corresponds to the off-shelf ball screw product that has 16 mm lead and 16 mm diameter. Screw ball-nut is mounted inside our customized motor rotor for better concentricity and fewer components. The mixed usage of bearings reduces friction in the system, improving efficiency and also smoothing the starting torque.

The concept of a four-bar mechanism of the knee (or shank) actuator is illustrated in Fig. 3. The joint A angle α is defined as the angle between the link a and link d. The location of point B is determined by α and link a length l_a:

$$[x_B,\ z_B]^T = \begin{bmatrix} l_a \cos\alpha, & l_a \sin\alpha \end{bmatrix}^T \tag{1}$$

[1]Motor drive hardware design file is hosted at `https://github.com/horychen/ProjectEureka` and its corresponding firmware is hosted at `https://github.com/horychen/ProjectPanGu-C`. The Webots simulation and environment files for Cury are hosted at `https://github.com/horychen/CuryLegWebotSimulation`.

[2]The lead of the screw is 16mm and the diameter of the screw is 16mm.

[3]Stator diameter is 130 mm, active axial length is 16 mm, and speed per voltage ratio is 20 rpm/V.

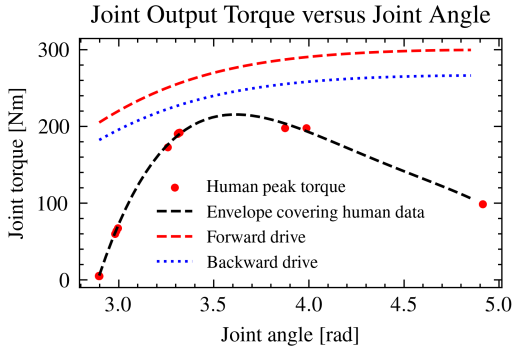

Fig. 4. Comparison between linear actuator joint output torque and the envelope of the peak joint torque of a real human while walking. Here, the envelope of the human data serves as the requirement for the joint actuator design for a human-size bipedal robot.

The distance $\mathrm{OC} = l_e$ between point O and point C is related to Θ by the parameters of ball screw and rod end:

$$l_e(\Theta) = \frac{\Theta}{2\pi} l_{\mathrm{bs}} + \mathrm{offset} \tag{2}$$

where $l_{\mathrm{bs}} = 16$ mm is the ball screw lead length, and the value offset is the initial distance considering the rod end length. Finally, the relation between the motor angular position Θ and α can be solely determined by solving through the geometric equations as follows:

$$\begin{cases} [x_B(\alpha) - x_C]^2 + [z_B(\alpha) - z_C]^2 = l_b^2 \\ (x_D - x_C)^2 + (z_D - z_C)^2 = l_c^2 \\ (x_O - x_C)^2 + (z_O - z_C)^2 = l_e(\Theta)^2 \end{cases} \tag{3}$$

C. Torque Requirement

Our design specification for the actuator torque required for bipedal robot walking is based on human walking data collected across different step widths, speeds, and lengths [17]. The actuator torque requirement is rendered as the envelope of human walking data in Fig. 4 with an additional safety factor of 1.13. Also shown in Fig. 4 are the analytical calculation results of the joint output torque of our linear actuator used in Cury. The joint output torque is different when the joint is pushed forward and backward, as the transmission efficiency is assumed to be 90% for forward drive and 80% for backward drive. It can be concluded that our linear actuator with the adopted motor is able to cover both the required joint moving range and required the joint torque, without needing any gearbox, hence having potential for better backdrivability.

To find a mechanical design that satisfies the joint torque requirement, multi-objective optimization (MOO) is performed to determine the lengths l_a, l_b, l_c, l_d for four-bar linkages and motor frame holder location OD. The algorithm we use is the MOEA/D algorithm implemented by PyGMO [23]. The three objectives are established to minimize the maximal torque requirement, total mass, and the distance OD between point O to point D. The mass is calculated by assuming the link is of uniform density. Since the link d is fixed and attached to the leg structural frame, it is safe to set its mass per length value to be 0. The objective on distance OD is used to keep motor close to the center of the

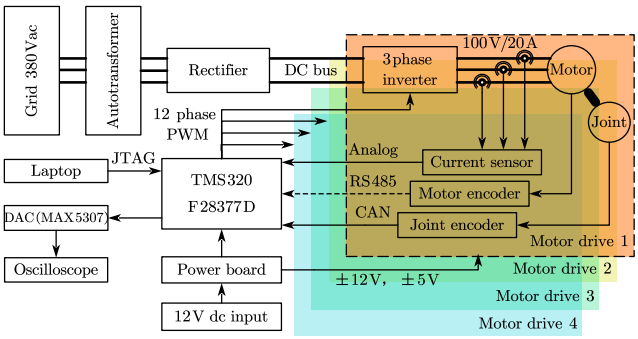

Fig. 5. The block diagram of motor drive with one micro controller and four three phase drivers. The communication protocol is marked next to the corresponding line. dc voltage of 12V is supplied via an auxiliary power source for the microcontroller and sensors.

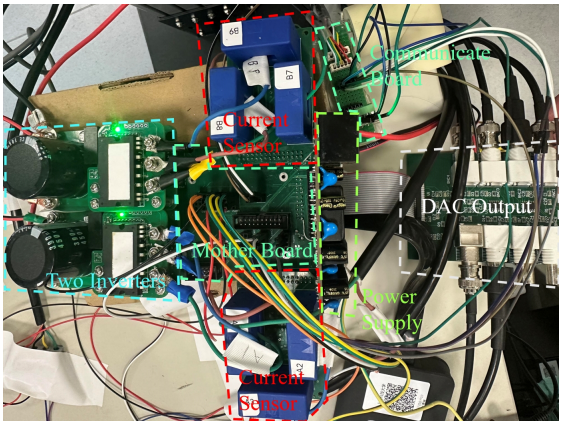

Fig. 6. Photo of the motor drive with two three-phase inverters.

eg as an effort to limit the total volume of the leg. In fact, the optimization results show that a very high motor holder location (i.e., large OD value) is beneficial for reducing the need of the motor peak torque, but apparently high motor location makes the thigh section rather wide. Taking this into account, the selected values of the design variables of the optimized four bar mechanism and the corresponding search space are summarized in TABLE I.

D. Motor Drive Design

To provide enough power for selected motors and simplify the system, the motor drive, as shown in Fig. 5, is customized. The digital signal processor (DSP) is chosen as Texas Instruments TMS320F28377D with a BGA footprint, which is capable of controlling up to four three-phase motor drive units and sending the signal to the DAC (digital-to-analog converter) extension board at the same time. The DAC is implemented using MAX5307 and generates real time waveform of the motor to be captured by the oscilloscope. Each of the motor drive units receives feedback signals from:

- three current sensors with current source analog output;
- one 23-bit motor encoder following the Tamagawa protocol via RS485;
- one 17-bit joint encoder via controller area network;
- dc bus voltage as analog signal;

TABLE I

OPTIMIZATION SETUP FOR FOUR BAR MECHANISM

Parameter	Symbol	Mass per length [g/mm]	Range [mm]	Selected value [mm]
Length of link a	l_a	2.18	[50,100]	80
Length of link b	l_b	1.61	[100,200]	133.98
Length of link c	l_c	0.57	[100,200]	153.07
Length of link d	l_d	0.0	[50,100]	52.28
x-coordinate of motor holder	x_O		[150,200]	110.76
z-coordinate of motor holder	z_O		[100,200]	192.03

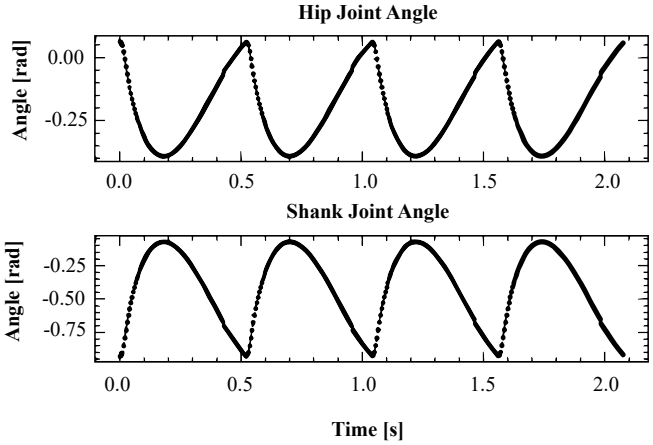

Fig. 7. Simulated joints angles of shank and hip over time.

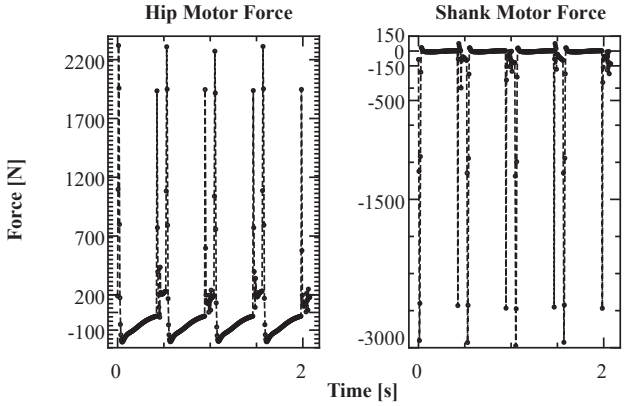

Fig. 8. Simulated motor force applied at rod end over time, i.e., the thrust force applied at point C in Fig. 3.

and sends pulse width modulation (PWM) signals to a three-phase inverter (FairChild FNC42060), which controls the motor terminal voltages.

Compared with the off-shelf product, our customized motor drive needs only one microprocessor and is able to control up to four three-phase inverters, eliminating the need to communicate among microprocessors. This potentially simplifies the robot system, reduces the cost of motor drives, and reduces control delay. The DSP collects all sensor signals for all four motor drive units, facilitating direct coordination and control among lower-level joints. The entire hardware, as shown in Fig. 6, is divided into multi-boards, which allows users to meet their special needs by replacing fewer parts of the hardware.

III. SIMULATION RESULTS AND CONTROL ARCHITECTURE

A. Closed-Loop Chain Dynamics Simulation

Given that most of the dynamics libraries and simulators lack proper support for closed-loop dynamic and there are limited choices on file types when exporting from popular design software such as SolidWorks, the mainstream methods for simulating systems with closed-loop chains [6], [24], [25]. are now briefly discussed.

To simulate the robot system and its closed chains, additional force equality constraints can be incorporated or virtual joints can be utilized.[4] Introducing force equality constraints in the simulators necessitates additional adjustments to the parameters of the elastic model and solver. This process demands significant effort to fine-tune the parameters, as selecting inappropriate values may lead to incorrect energy changes at the joints or the inability to establish rigid connections. However, the inclusion of virtual joints in the model offers a way to simplify it by approximating the closed-loop chain. Nonetheless, this approach needs manually model and approximation of the closed-loop chains bringing extra errors to the model.

This paper adopts Webots to simulate robot system, for it offers the node called "SolidReference" that supports closed-loop chain dynamics and precise modeling with automatic model parameter setup capability. After obtaining URDF file from SolidWorks, it can be transferred to "PORTO" format through the official tool[5] and the closed-loop chain dynamics can be easily realized by changing node type.

B. Simulation Result

In our simulation environment, Cury is positioned on a hidden bench and is capable of vertical movement. The objective of the simulation is to evaluate the predefined trajectory illustrated in Fig. 7, which allows Cury for making small jumping through positional tracking, and to determine if the actuators meet the specified trajectory requirements. The model is simplified in a sense that the ball screw is not modelled so the actuator input is the thrust or pulling force applied to the end of the ball-screws. Based on Fig. 8, we can confirm that the actuators meet the output requirement to perform the leg movement.

[4]Virtual joint mentioned can be found at `https://github.com/pal-robotics/gazebo/ros/link/attacher`.

[5]The official tool for transferring URDF to PORTO is hosted at `https://github.com/cyberbotics/urdf2webots`

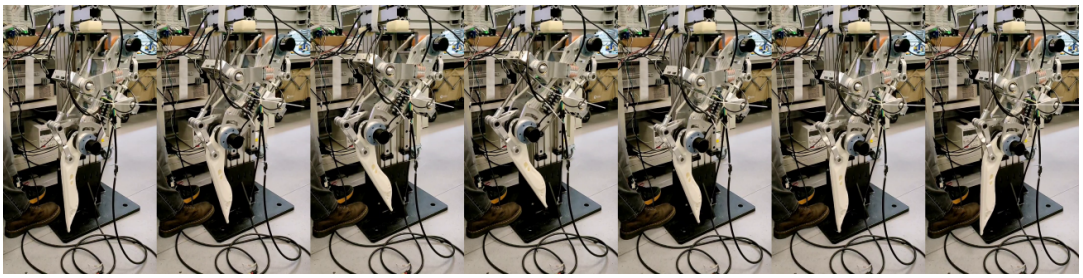

Fig. 9. Sequential snapshot of one cycle during the leg trajectory tracking.

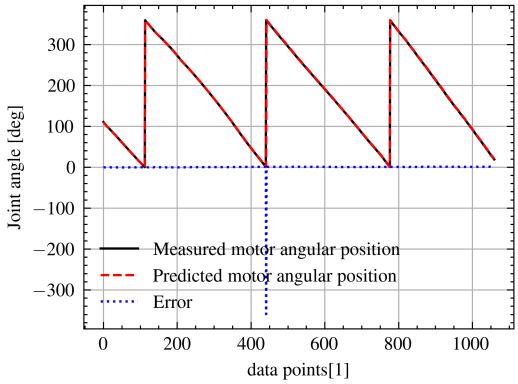

Fig. 10. Predicted motor angular position using joint position.

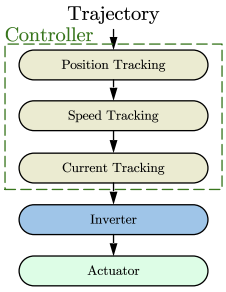

Fig. 11. Control diagram in experiment

IV. Experimental Results

Cury, the leg prototype, is fixed to a slider on a vertical test bench, repeating the given predefined trajectories of the two joints, and the sequential snapshot of a single cycle is shown in Fig. 9.

A. Kinematics Analysis

To verify the kinematic formulations and mechanical performance, the angle of shank joint is used as example for predicting the motor angular position using the equation shown in (1)–(2) and then compared with data collected from the motor encoder. as shown in Fig. 10, one can see that motor angular position can be accurately predicted with only knowing the angular position of joint in most points. The impulse error 360 deg observed in the middle of the image is attributed to a minor deviation compounded by the motor that completes one full rotation. Moreover, since the predicted joint angle in Fig. 10 is calculated based on the joint encoder, it is essentially an open-loop prediction, which further implies that there is only minor clearance in the joint and actuator design, and this is a highly desired feature for a QDD joint. Additionally, Cury is quite backdrivable by a hand of an adult, as shown in the supplementary video. The above fact suggests a possible elimination of either joint encoder or motor encoder, reducing the complexity of the robot system.

B. Motion Tracking Test

The tracking controller is shown in Fig. 11. It receives two joint angle trajectory signals and send to trajectory tracker (a proportional controller) connecting with speed controller and current controller. The output of the entire controller consists of control signals for the inverter's switching transistors. The control process is processed inside the DSP with a update frequency of 10 kHz. The results of a motion tracking test is shown in Fig. 12. The tracking errors of both joints are relatively small, sufficient to allow the system to complete the specified trajectory. As can be seen from Fig. 12, the shank joint has a higher tracking error than the hip joint because the motor speed is limited by either the DC bus voltage or the position controller output limit. The phase current (from the hip motor) needed to complete the test is less than 2 A because the leg is tested in mid-air so the motor does not need too much torque to accomplish the trajectory tracking.

V. Conclusion and Future Work

This paper presents the design, simulation, and experimental results of a 2-DoFs leg prototype. Four-bar mechanisms and the corresponding multi-objective optimization for design parameter selection are presented. The selected design is able to support the human waling motion. To simulate the system containing closed-loop chain dynamics, an open-sourced simulation environment based on Webots is provided. In the simulator, a predefined trajectory is given for evaluating and testing the torque requirement of the actuators. The experiments and supplementary videos validate the design's characteristic of having a small clearance and backdrivability, as the motor angle positions can be accurately predicted based on joint positions and vice versa, and the specified trajectory can be executed effectively through a simple controller. An open-sourced motor drive is designed with a focus on enhancing system scalability and, at the same time, minimizing system complexity.

Future work includes leg control using one joint encoder (or one motor encoder), precise vertical jumping trajectory through optimization and control, and an iteration of the mechanical and electrical designs of the robot system.

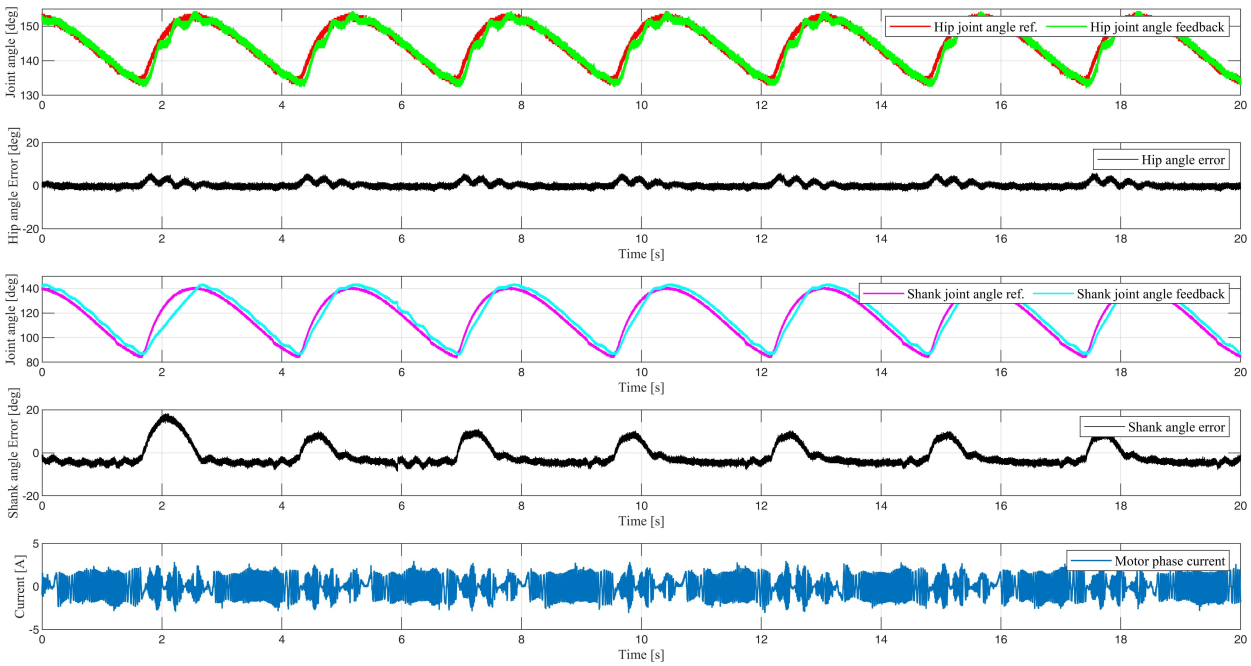

Fig. 12. Two joint motion tracking test results. At $t = 4$ s, the output limit of position control is increased from 300 r/min to 400 r/min, resulting in an improvement in position tracking of the shank joint after $t = 4$ s.

REFERENCES

[1] U. Robotics, "Unitree general-pupose humanoid robot h1 evolution v2.0," Nov. 2023. [Online]. Available: https://www.youtube.com/watch?v=q8JMX6PGRoI

[2] M. Chignoli, D. Kim, E. Stanger-Jones, and S. Kim, "The mit humanoid robot: Design, motion planning, and control for acrobatic behaviors," 2021.

[3] J. P. Reher, A. Hereid, S. Kolathaya, C. M. Hubicki, and A. D. Ames, *Algorithmic foundations of realizing Multi-Contact Locomotion on the humanoid robot DURUS*. Springer International Publishing, 2020, p. 400–415. [Online]. Available: https://link.springer.com/chapter/10.1007/978-3-030-43089-4_26

[4] B. Dynamics, "Atlas gets a grip," Jan. 2023. [Online]. Available: https://www.youtube.com/watch?v=-e1_QhJ1EhQ

[5] W. contributors, "Optimus (robot)," Jun. 2024. [Online]. Available: https://en.wikipedia.org/wiki/Optimus_(robot)

[6] S. Sovukluk, J. Englsberger, and C. Ott, "Highly maneuverable humanoid running via 3d slip+foot dynamics," *IEEE Robot. Autom. Lett.*, vol. 9, no. 2, 2024.

[7] Y. Sakagami, R. Watanabe, C. Aoyama, S. Matsunaga, N. Higaki, and K. Fujimura, "The intelligent asimo: System overview and integration," in *IEEERSJ Int. Conf. Intell. Robots Syst.*, vol. 3, 2002.

[8] G. Pratt and M. Williamson, "Series elastic actuators," in *Proc. 1995 IEEERSJ Int. Conf. Intell. Robots Syst. Hum. Robot Interact. Coop. Robots*, vol. 1, 1995.

[9] F. Cursi, W. Bai, E. M. Yeatman, and P. Kormushev, "Model learning with backlash compensation for a tendon-driven surgical robot," *IEEE Robotics and Automation Letters*, vol. 7, no. 3, pp. 7958–7965, 2022.

[10] Q. Tian, P. Flores, and H. M. Lankarani, "A comprehensive survey of the analytical, numerical and experimental methodologies for dynamics of multibody mechanical systems with clearance or imperfect joints," *Mechanism and Machine Theory*, vol. 122, 2018.

[11] G. Kenneally, A. De, and D. E. Koditschek, "Design principles for a family of direct-drive legged robots," *IEEE Robot. Autom. Lett.*, vol. 1, no. 2, 2016.

[12] G. Bledt, M. J. Powell, B. Katz, J. Di Carlo, P. M. Wensing, and S. Kim, "Mit cheetah 3: Design and control of a robust, dynamic quadruped robot," in *2018 IEEERSJ Int. Conf. Intell. Robots Syst. IROS*, 2018.

[13] Y. Ding and H.-W. Park, "Design and experimental implementation of a quasi-direct-drive leg for optimized jumping," in *2017 IEEERSJ Int. Conf. Intell. Robots Syst. IROS*, 2017.

[14] N. Kau, A. Schultz, N. Ferrante, and P. Slade, "Stanford doggo: An open-source, quasi-direct-drive quadruped," in *2019 Int. Conf. Robot. Autom. ICRA*, 2019.

[15] S. Feng, Y. Gu, W. Guo, Y. Guo, F. Wan, J. Pan, and C. Song, "An overconstrained robotic leg with coaxial quasi-direct drives for omnidirectional ground mobility," in *2021 IEEE Int. Conf. Robot. Autom. ICRA*, 2021.

[16] Y. Muraki, M. Ae, H. Koyama, and T. Yokozawa, "Joint torque and power of the takeoff leg in the long jump," *International Journal of Sport and Health Science*, vol. 6, 2008.

[17] T. J. van der Zee, E. M. Mundinger, and A. D. Kuo, "A biomechanics dataset of healthy human walking at various speeds, step lengths and step widths," *Sci Data*, vol. 9, no. 1, 2022.

[18] S. D. Potter, Z. J. Jackowski, A. Young, and B. D. Inc, "Us11754155b2 - screw actuator for a legged robot." [Online]. Available: https://patents.google.com/patent/US11754155B2/en

[19] B. Siciliano and O. Khatib, Eds., *Springer Handbook of Robotics*, ser. Springer Handbooks. Springer International Publishing, 2016.

[20] O. Michel, "Cyberbotics ltd. webots™: Professional mobile robot simulation," *Int. J. Adv. Robot. Syst.*, vol. 1, no. 1, 2004.

[21] M. E. Carney, T. Shu, R. Stolyarov, J.-F. Duval, and H. M. Herr, "Design and preliminary results of a reaction force series elastic actuator for bionic knee and ankle prostheses," *IEEE Trans. Med. Robot. Bionics*, vol. 3, no. 3, 2021.

[22] "Pan motor." [Online]. Available: http://pan-motor.com/page/en-index.html

[23] F. Biscani and D. Izzo, "A parallel global multiobjective framework for optimization: pagmo," *Journal of Open Source Software*, vol. 5, no. 53, p. 2338, 2020. [Online]. Available: https://doi.org/10.21105/joss.02338

[24] S. Sovukluk, J. Englsberger, and C. Ott, "Whole body control formulation for humanoid robots with closed/parallel kinematic chains: Kangaroo case study," in *2023 IEEERSJ Int. Conf. Intell. Robots Syst. IROS*, 2023.

[25] A. Roig, S. Kishor Kothakota, N. Miguel, P. Fernbach, E. Mingo Hoffman, and L. Marchionni, "On the hardware design and control architecture of the humanoid robot kangaroo," in *6th Workshop Legged Robots Int. Conf. Robot. Autom. ICRA*, 2022.